Colloid Polym Sci 278:211–219 (2000)

ORIGINAL CONTRIBUTION

J. Németh
I. Dékány

The effect of nanoparticle growth on rheological properties of silica and silicate dispersions

Received: 20 July 1999
Accepted in revised form: 22 September 1999

J. Németh · I. Dékány (✉)
Department of Colloid Chemistry
University of Szeged and Nanostructured Materials Research Group of the Hungarian Academy of Science
H-6720 Szeged, Aradi V.t.1., Hungary
e-mail: i.dekany@chem.u-szeged.hu
Tel.: +36-62-544210
Fax: +36-62-424646

Dedicated to 60th birthday of Professor Gerhard Lagaly

Abstract CdS and ZnS nanoparticles were prepared in the solid–liquid interfacial adsorption layer as a nanophase reactor. The substrates were hydrophilic and hydrophobic aerosils and hydrophilic layer silicates dispersed in ethanol–cyclohexane mixtures. The growth of particles at various surface concentration of precursor ions was monitored by absorption spectroscopy, band-gap-energy measurements and particle diameter measurements. Also, the rheological properties of nanoparticle–support composites in organic and aqueous dispersions were measured. The energy of separation between the nanoparticles depended on the particle diameter. The intercalation of nanoparticles in the layered silicates yielded a nanostructured two-phase system. The presence of semiconductive subcolloids was proven by transmission electron microscopy measurements, which offer an excellent possibility for the determination of the particle size distribution.

Key words Nanophase reactors · Nanoparticles · CdS · ZnS · Aerosils

Introduction

Research on systems at the lower limit of the colloidal size range – of nanometre dimensions – and the development of methods for producing such systems were, for some time, at the centre of interest. The first important results were published by Henglein [1], who pointed out that nanostructured colloidal systems had been referred to by Ostwald [2] in a book published as early as 1916. The reason for this intense interest is the fact that particles in this size range possess novel and often very special properties, opening the way to many new and exciting practical applications [3–9].

The aim of the present work was the synthesis of semiconductor particles (CdS and ZnS) of controlled size which approached the lower limit of colloidal size (i.e. diameters of a few nanometres) and the examination of their physical properties. From the large variety of suitable semiconductors (TiO_2, ZnO, SnO_2, CdS, ZnS, etc.) sulphide compounds were chosen for this study, because these can be produced by relatively simple reactions [10–12]. We aimed at identifying conditions for synthesis which do not require the addition of surfactants for stabilization of the particles. For this aim controlled synthesis was realized on the surface of SiO_2-based spherical supports or layer silicates. The support itself acted as a stabilizer, and the synthesis proceeded in a suspension. The solid–liquid interfacial adsorption layer functioned as a nanophase reactor [13–15].

Monodispersity of particles and stabilization are very important criteria in controlled synthesis. Particle growth must be stopped at a small size by cutting off the supply of reagent. For this reason, very low concentrations (10^{-3}–10^{-4} mol/dm^3) are used and a stabilizing agent must be added to preserve monodispersity. The systems serving to control particle growth are themselves nanostructured (micelles, microemulsions, interlamellar space of clay minerals, etc.), just like the particles to be synthesized. The procedures most widely used are described below.

A common way to achieve a uniform particle size is to carry out the synthesis in the interior of microemul-

sion liquid droplets [6, 16–18]. For example, metallic palladium nanoparticles were produced in microemulsions by combining adequate amounts of organic solvent, water and surfactant, a precursor of Pd^{2+} ions and reducing agents, for example, hydrazine. One disadvantage of this method lies in its expensiveness due to the necessity of adding large amounts of surfactant (as much as 20–30%) to the system. Another drawback is that the surfactant ensuring colloid stability is adsorbed on the surface of the nanoparticles, thereby decreasing their catalytic activity. The disadvantages may be circumvented by the application of micellar synthesis, in the course of which the desired reaction takes place in the interior of the micelle. When long-chain surfactants are used, micelles with diameters of 2–10 nm are formed which incorporate substantially less surfactant than with the previous method. Nanoparticles are generally produced in inverse micelles; however, semiconductor particles [6, 16] and even homogeneous $Zn_xCd_{1-x}S$ mixed crystals [17] were obtained and stabilized in micelles. Again, the particles are stabilized by the surfactant adsorption layer, as in the case of the microemulsion procedure; however, the presence of this layer can also lead to complications [18, 19]. For example, blockage of the active sites of the synthesized nanoparticles by surfactant molecules interferes with their utilization as a catalyst.

The most obvious way to circumvent the above-mentioned problems is to avoid the use of surfactants. Particle synthesis may be controlled by two-dimensional structures, for example, the layers of clay minerals [20–23]. These themselves are nanostructured systems and their lyophilicity and basal spacing can be modified by the incorporation of alkyl chains. The monodispersity of nanoparticles grown in the interlamellar space is attained by stopping the supply of reagent; otherwise, the increasing voluminous particles of various sizes will push the lamellae apart [15–20].

An even simpler system is obtained when the synthesis is allowed to proceed in the adsorption layer created on the surface of the dispersed particles [14, 15, 20–23]. The conditions for creating such a system are as follows.

1. One liquid component is preferentially adsorbed on the solid surface and, consequently, its concentration in the bulk phase is close to zero ($x_1^s \gg x_1$).
2. The reaction partners are highly soluble in the preferentially adsorbed component, allowing the delivery of sufficient amounts of reactants to the adsorption layer.
3. The second liquid component is not adsorbed on the interface ($x_2 \gg x_2^s$) and the solubility of the reactants in this component is close to zero.

For synthesis, the appropriate reagent is added to the disperse system (most often a suspension) and the chemical reaction takes place within the adsorption layer of the suspended particles; the size of the nanoparticles is controlled by adjusting the thickness of the adsorption layer. The advantage of this method is that the synthesized catalyst particles do not have to be transferred to the surface of the support at a later time. The procedure may be further simplified if the nanophase reactor is formed of alcohols which react with the precursor ions as a reducing agent and the reaction starts immediately after the addition of metal ions. If, for example, the dispersing medium is a binary mixture of ethanol and cyclohexane in which SiO_2 particles are dispersed, ethanol forms an adsorption layer on the surface of the SiO_2 particles; when palladium(II) acetate is added to the system, metal ions move to the more polar interfacial adsorption layer, where they are immediately reduced to metallic palladium by the preadsorbed ethanol. However, a disadvantage of this procedure is that in the absence of a stabilizing agent the suspension may undergo recrystallization or coarsening and the particle size may increase if the particles remain suspended at all. Particles of unchanged size can be obtained by immediate drying and storage.

Experimental

Materials

CdS and ZnS nanoparticles were synthesized in the solid–liquid interfacial adsorption layer. The supports were suspended in binary mixtures of organic solvents. The dispersion medium was an ethanol–cyclohexane mixture in which the mole fraction of ethanol was 0.05.

The suspended particles were spherical, hydrophilic SiO_2 (A200), hydrophobic SiO_2 (R972, Degussa, Germany), Optigel (soda-activated bentonite, Süd-Chemie, Germany) and Laponite (synthetic hectorite, Laport, UK). The concentration of the suspension was 1 g/100 cm^3 ethanol–cyclohexane.

The reagents were cadmium(II) acetate, zinc(II) acetate and sodium sulphide, dissolved in ethanol. The concentration of the precursor ions was 1–5 mmol/dm^3.

Methods

Sample preparation

The following reactions occur on the surface of support materials in the adsorption layer enriched in ethanol:

$$(CH_3COO)_2Cd + Na_2S \rightarrow CdS + 2CH_3COONa$$
$$(CH_3COO)_2Zn + Na_2S \rightarrow ZnS + 2CH_3COONa$$

For each support, four different precursor ion concentrations were used: $c_{Zn\ or\ Cd} = 0.05$, 0.5, 5 and 50 μmol/g support.

For calculations of the composition of the solvent mixture, the ethanol content of the reagents was also taken into account, and so the resulting molar fraction of ethanol was 0.05. Supports were first suspended in cyclohexane. After the addition of a calculated amount of cadmium or zinc acetate dissolved in ethanol, the suspension was homogenized by sonication. The precursor ions were adsorbed on the surface of the support particles over a period

of 24 h. As soon as a calculated amount of the adequately diluted Na_2S solution was added to the vigorously stirred dispersion, the reaction took place immediately.

Since Optigel and Laponite are markedly hydrophilic, they settle rapidly; this would seriously interfere with further measurements. In order to prevent this, the system containing the nanoparticles was redispersed in water after evaporation of the organic dispersion medium. Stable dispersions suitable for further measurements (rheology, UV-Vis spectrophotometry) were obtained. X-ray diffraction (XRD) experiments were conducted on powdered samples.

Spectrophotometry

Spectrophotometric measurements are based on the phenomenon that light of suitable wavelengths is absorbed by the nanoparticles, leading to the excitation of their electrons. The energy difference (E_g), between the valence band and the conduction band is inversely proportional to the particle size. With decreasing particle size, the absorption edge shifts towards smaller wavelengths. The band-gap energy, E_g, is calculated from the wavelength, λ_g, at the absorption edge using Eq. (1):

$$E_g = h\,c/\lambda_g \quad , \tag{1}$$

where h is the Planck constant, c is the velocity of light and λ_g is the wavelength of the absorption edge. The particle diameter, d_p, is calculated from E_g using the Brus equation [11, 24]:

$$E_g = E_{g,bulk} + \frac{h^2}{2d_p^2}\left(\frac{1}{m_e}+\frac{1}{m_h}\right) - \frac{3.6e^2}{4\pi\varepsilon d_p} \tag{2}$$

and

$$d_p = \frac{\frac{3.6e^2}{4\pi\varepsilon} - \sqrt{\left(\frac{3.6e^2}{4\pi\varepsilon}\right)^2 - 4(E_{g,bulk}-E_g)\;\frac{h^2}{2}\left(\frac{1}{m_e}+\frac{1}{m_h}\right)}}{2(E_{g,bulk}-E_g)} \quad , \tag{3}$$

where $E_{g,bulk}$ is the band-gap energy of the semiconductor in the bulk phase, m_e is the effective mass of an electron in the semiconductor, m_h is the effective mass of a hole in the semiconductor, e is the charge of an electron and ε is the dielectric constant of the semiconductor. Spectra were recorded using UVIKON 930 UV-Vis dual-beam spectrophotometer at 25 ± 0.1 °C. A sample of the dispersed support of identical concentration, free of nanoparticles, served as a reference.

Rheological measurements

Rheological measurements of the suspensions were carried out with a Haake RV20-CV100 computer-controlled rotational viscosimeter (ME-15 measuring head) at 25 ± 0.1 °C.

XRD measurements

The aim of the XRD measurements on systems containing the silicate supports was to detect structural changes brought about by the nanoparticles formed. Measurements were made using a Philips PW1820 diffractometer (Cu Kα, 40 kV, 35 mA). The accuracy of the d_L values was ±0.01 nm.

Transmission electron microscopy

Transmission electron microscopy (TEM) pictures were taken using an OPTON 902 electron microscope, using a voltage of 100 kV. Samples were suspended in ethanol and spread on copper grids coated with Formwar foil.

Results and discussion

Determination of particle size by spectrophotometry

Experiments on the synthesis of CdS nanoparticles were started with the hydrophilic aerosil A200 in ethanol–cyclohexane with a mole fraction of ethanol of 0.05.

The preferentially adsorbed ethanol forms an adsorption layer on the surface of the SiO_2 particles. The reason why a molar fraction of 0.05 was chosen for ethanol in ethanol–cyclohexane was that, according to the evidence of liquid sorption experiments, the selectivity is a maximum at an ethanol of mole fraction of 0.05–0.1 [26–28].

The absorption spectra reveal that the absorption edge is shifted to shorter wavelengths with decreasing concentrations (and particle sizes) (Fig. 1). Also, the absorption intensity decreases with decreasing precursor ion concentration since fewer particles are formed. Stepwise light absorption occurs in the visible range at about 500 nm at the highest concentration of precursor, at about 440 nm in system B and at around 350 nm in systems C and D (Fig. 1). These results agree with the observation that system A is yellow while, due to the blue shift, the other systems do not display this colour. The formation of ZnS nanoparticles is not accompanied by a change in colour (Fig. 2). The characteristic spectra are similar to those of the systems containing CdS; however, when nanoparticles are synthesized on the hydrophobized SiO_2 (R972), the character of the spectra changes slightly.

In the presence of Optigel, the particles are expected to be formed in the interlamellar space; however, at

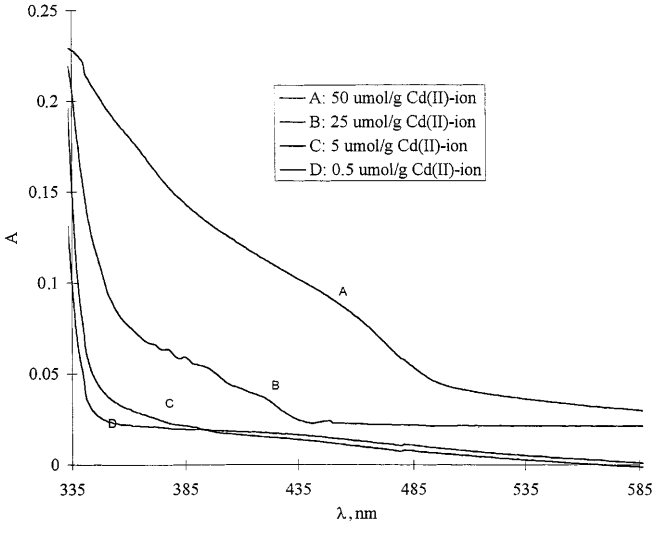

Fig. 1 Absorption spectra of CdS nanoparticles on Aerosil 200 at various surface precursor ion concentrations

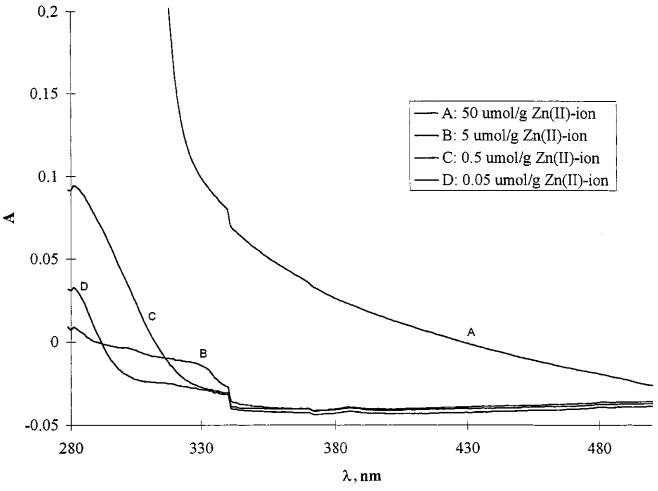

Fig. 2 Absorption spectra of ZnS nanoparticles on Aerosil 200 at various surface precursor ion concentrations

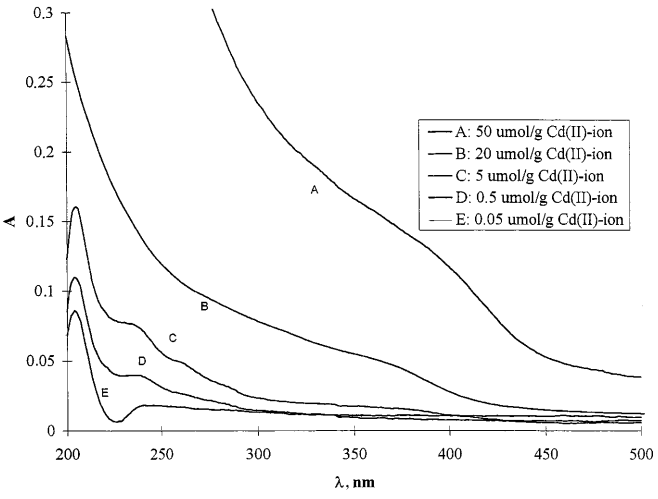

Fig. 3 Absorption spectra of CdS nanoparticles on Optigel at various surface precursor ion concentrations

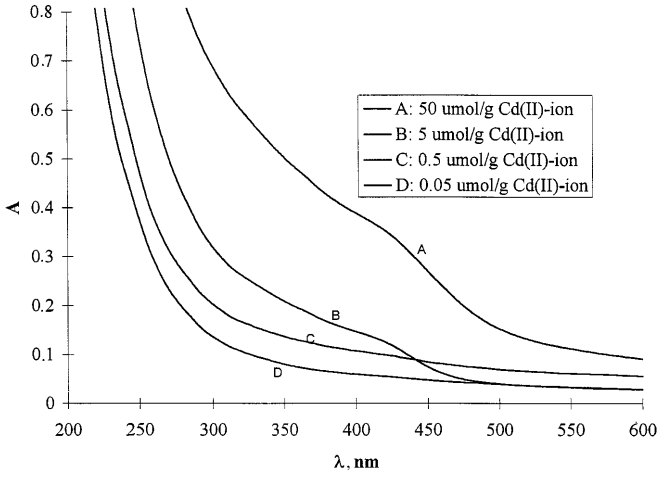

Fig. 4 Absorption spectra of CdS nanoparticles on hectorite at various surface precursor ion concentrations

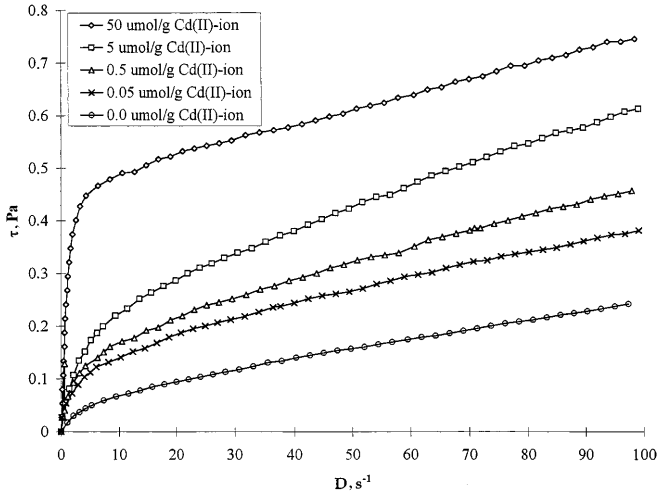

Fig. 5 Flow curves of CdS/Aerosil R972 dispersions in ethanol–cyclohexane at an ethanol molar fraction of 0.05 at various surface precursor ion concentrations (only the increasing branch is shown)

higher concentrations (in systems A and B) larger particles may also be formed – mostly in the bulk phase – according to the evidence of the spectra (Figs. 3, 4). The formation of larger particles is explained by the onset of particle growth in the bulk phase at higher concentrations, yielding a coarse precipitate with particle sizes in the micro range. It may also occur that particles formed on the solid surface continue to grow or that primary particles form large clusters on the surface. Similar spectra are shown by ZnS nanoparticles formed on Laponite, they are also similar to those of the CdS nanoparticles.

The data reveal a direct proportionality between the number of ions delivered to the adsorption layer or the interlamellar space during synthesis and the diameter of the nanoparticles (Tables 1, 2). Larger particles are generated at higher concentrations, indicated by an increase in the wavelengths, λ_g, and, consequently, by a decrease in the energy of the band gap. This behaviour is also illustrated in Table 1.

Detectable amounts of nanoparticles are formed only in the concentration range 10^{-5}–10^{-8} mol precursor/(g support) because aggregates of larger particle size are formed at higher concentrations, while at lower concentrations subcolloidal structures are not formed at all due to extensive dilution. On the basis of the light absorption spectra nanoparticles are formed on every support, even on the surface of hydrophobized SiO_2, although on this support fewer and smaller particles were formed owing to weaker ion adsorption (Table 1).

Table 1 Analysis of absorption spectra of ZnS nanoparticles on different supports at various surface concentrations

c_{ZnS}(μmol/g)	0.05	0.5	5	50
Hydrophobic SiO_2 (R 972) a^s = 140 m^2/g				
λ_g (nm)	312.5	318.1	319.4	330.6
d_p (nm)	4.1	4.5	4.7	6.5
Hydrophilic SiO_2 (A 200) a^s = 200 m^2/g				
λ_g (nm)	291.7	319.4	340.3	329.2
d_p (nm)	3.1	4.7	Bulk	6.0
Optigel a^s = 750 m^2/g				
λ_g (nm)	287.0	292.1	310.5	323.7
d_p (nm)	3.0	3.2	4.0	5.1
Laponite (hectorite) a^s = 800 m^2/g				
λ_g (nm)	332.1	332.6	344.0	350.9
d_p (nm)	7.1	7.1	Bulk	Bulk

Table 2 Analysis of absorption spectra of CdS nanoparticles on different supports at various surface concentrations

c_{CdS}(μmol/g)	0.05	0.5	5	50
Hydrophobic SiO_2 (R 972) a^s = 140 m^2/g				
λ_g (nm)	315.9	319.5	330.5	342.7
d_p (nm)	2.3	2.4	2.5	2.6
Hydrophilic SiO_2 (A 200) a^s = 200 m^2/g				
λ_g (nm)	339.5	340.2	342.4	492.4
d_p (nm)	2.5	2.6	2.6	9.0
Optigel a^s = 750 m^2/g				
λ_g (nm)	214.5	281.6	290.8	436.8
d_p (nm)	1.6	2.0	2.1	4.2
Laponite (hectorite) a^s = 800 m^2/g				
λ_g (nm)	273.1	275.4	465.1	483.4
d_p (nm)	2.0	2.0	5.4	7.0

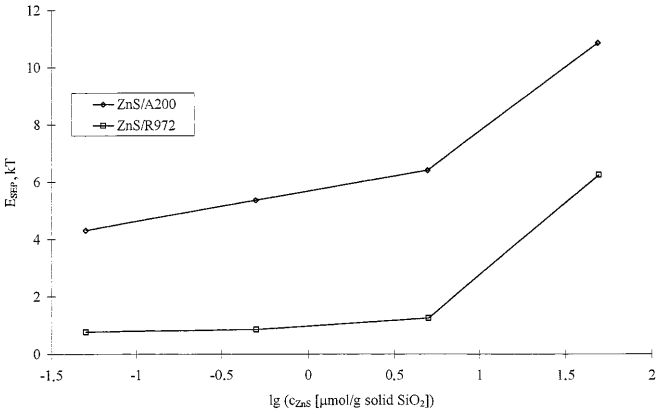

Fig. 6 Energy of separations of ZnS/aerosil particles in ethanol–cyclohexane at various surface precursor ion concentrations. Hydrophilic surface (*upper curve*), hydrophobic surface (*lower curve*).

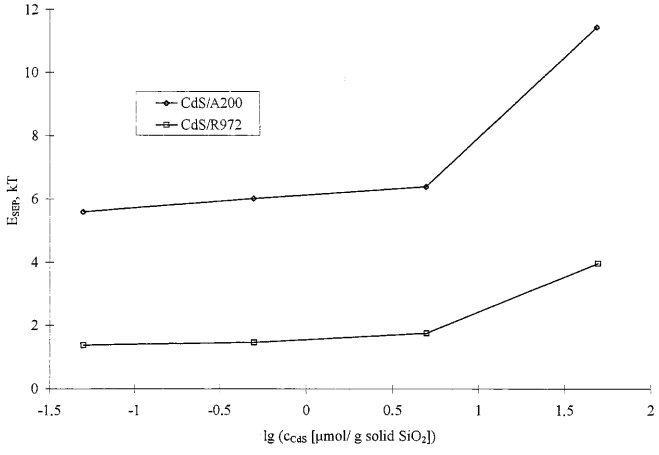

Fig. 7 Energy of seperation of CdS/aerosil particles in ethanol–cyclohexane at various surface precursor ion concentrations. Hydrophilic surface (*upper curve*), hydrophobic surface (*lower curve*)

Rheological measurements

The presence of nanoparticles changes the flow and the structure-building properties of the dispersions. The determination of viscosity yields valuable information on the interaction between the dispersed particles. The rheological behaviour of non-Newtonian fluids is usually characterized by the flow curves, $\tau = f(D)$, representing the shear stress (τ) as a function of the shear gradient (D). In the case of plastic and pseudoplastic systems nonlinear functions of $\tau = f(D)$ are obtained which are described by the relationship $\tau = \tau_B + \eta_{pl}D$. Extrapolation of the linear section of the flow curves to $D = 0$ gives the Bingham yield value, τ_B, while the slope yields the plastic viscosity, η_{pl}.[29]. If nanoparticles are formed in the system, they link the particles, thus creating an internal structure which increases the viscosity and the yield. From τ_B values the energy of separation of two particles (E_{SEP}) can be calculated [29]:

$$\tau_B = \frac{3\Phi^2}{2\pi^2 r^3} E_{SEP} \quad , \tag{4}$$

where τ_B is the Bingham yield value, Φ is the volume fraction of solid particles and r is the particle radius. The energy is expressed in units of kT where k is the Boltzmann constant (1.381×10^{-23} JK^{-1}) and T = 298.15 K (Figs. 6, 7).

Some characteristic flow curves are presented in Figs. 5, 8, 9. The presence of nanoparticles considerably increases the yield, parallel with the adsorbent precursor ion concentrations on the support surface. Even more powerful effects are observed when the surface of the support is not hydrophobized because the adhesion between the particles is higher (Fig. 8). Aqueous sus-

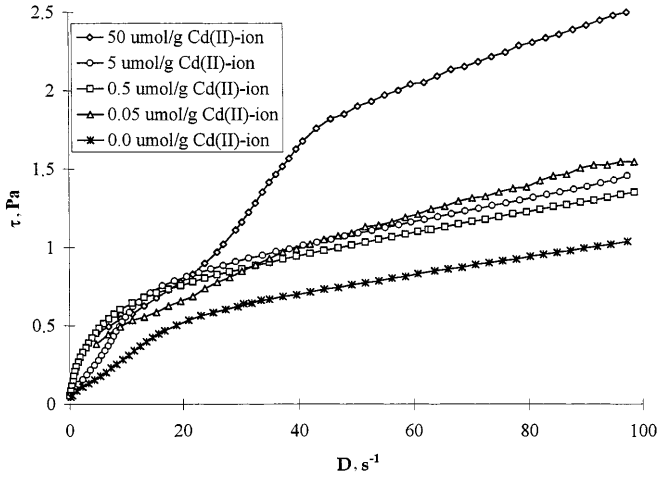

Fig. 8 Flow curves of CdS/Aerosil R972 dispersions in ethanol–cyclohexane at an ethanol molar fraction of 0.05 at various surface precursor ion concentrations (only the increasing branch is shown)

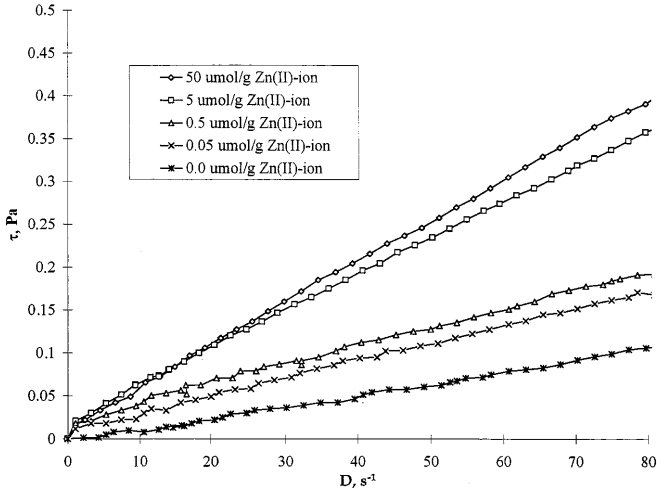

Fig. 9 Flow curves of ZnS/Optigel in aqueous dispersions at various surface precursor ion concentrations (only the increasing branch is shown)

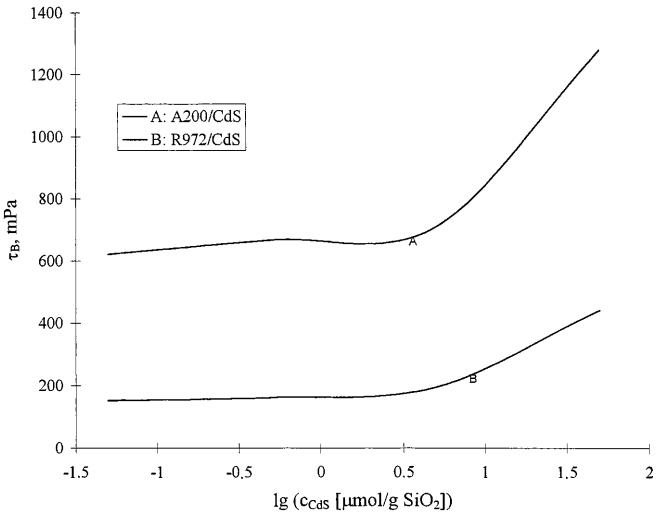

Fig. 10 Bingham yield values of CdS/aerosil dispersions in ethanol–cyclohexane at various surface precursor ion concentrations. Hydrophilic surface (*A*), hydrophobic surface (*B*)

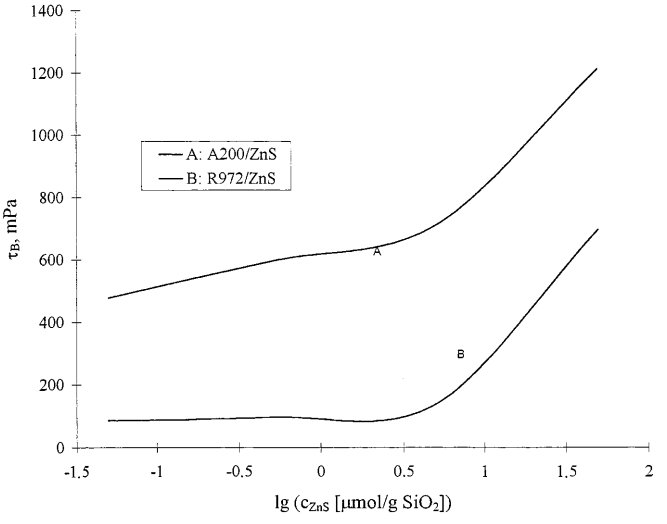

Fig. 11 Bingham yield values of ZnS/aerosil dispersions in ethanol–cyclohexane at various surface precursor ion concentrations. Hydrophilic surface (*A*), hydrophobic surface (*B*)

pensions of Optigel at pH 8.5 behave as Newtonian fluids (Fig. 9). The reason for this is that the particles are readily wetted in aqueous media and interparticle adhesion is minimal. Although these very dilute systems (1% solid content) do not show a yield value, the viscosity increases with increasing concentration (increasing slope of curves). The η–D functions also demonstrate the presence of a relatively ordered internal structure: at identical shear gradients higher concentrations are associated with higher viscosities. At low shear gradients (D = 0–5 s^{-1}), the viscosity is significantly increased, i.e. shearing orders the structure of the system in the direction of the shear. Evidently, there is minimal adhesion between the silicate lamellae and the nanoparticles. Changes in the yield values in the non-Newtonian systems are summarized in Figs. 10 and 11.

The behaviour of the separation energy, E_{SEP}, calculated with the help of τ_B and Φ (the volume fraction of the suspension) indicates that as the precursor ion concentration is increased an increasing amount of energy is necessary for the separation of the particles. The increase in viscosity in Newtonian systems and in both the yield value and the plastic viscosity in non-Newtonian systems is an unambiguous indication of the linking of suspended particles by the nanoparticles,

creating a new structure which can be adequately characterized by rheological parameters [20].

The properties of lamellar structures

XRD measurements were performed on powdered samples; Optigel was studied before and after the formation of ZnS nanoparticles (Fig. 12). Pure Optigel shows a broad peak in the range 0–15°, which corresponds to an average basal spacing of 1.4 nm. After reaction a new, sharp peak appears in the small-angle range, which indicates the intercalation of the nanoparticles in the layered structure. The original peak assigned to Optigel maintains its position. This is observed for all ZnS concentrations tested. The intensity of the new peak shows a tendency to increase with increasing concentration (Table 3). Thus, our studies verify the presence of nanoparticles of 4–5 nm in the interlamellar space. Particle size is not unambiguously correlated with the concentration since the final size is significantly influenced by the rate of seed formation and growth. Hectorite samples with CdS showed similar behaviour (Figs. 13, 14). As listed in Table 3, the basal spacing is significantly increased. The average interlamellar distance increases considerably, indicating that the particles remain in the interlamellar space. Nanoparticles disrupt the originally highly ordered lamellar structure by linking together less-ordered lamellar packets of smaller size as represented in Fig. 15.

Determination of particle size by TEM

The TEM pictures clearly show the presence of nanoparticles. These pictures can also be used for the construction of particle size distribution functions. The particles of the suspensions containing nanoparticles were dried and redispersed in ethanol before being photographed. The particle size increased as a result of this pretreatment: even sonication failed to disperse homogeneously the particles which adhered to each other, forming small aggregates. Some representative pictures are shown in Figs. 16, 17. According to these

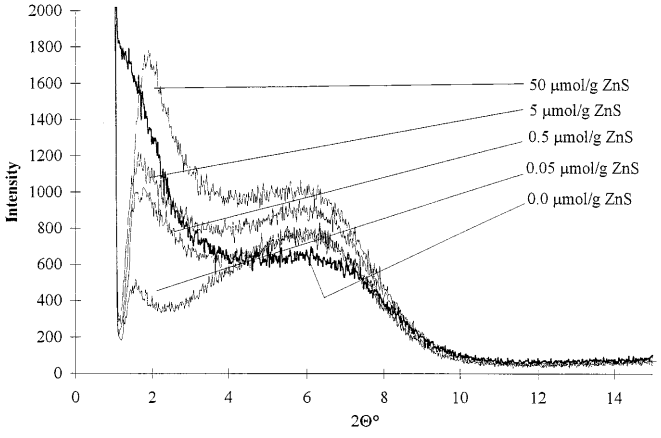

Fig. 12 X-ray diffraction (*XRD*) pattern of ZnS/Optigel nanocomposite powder at different surface precursor ion concentrations

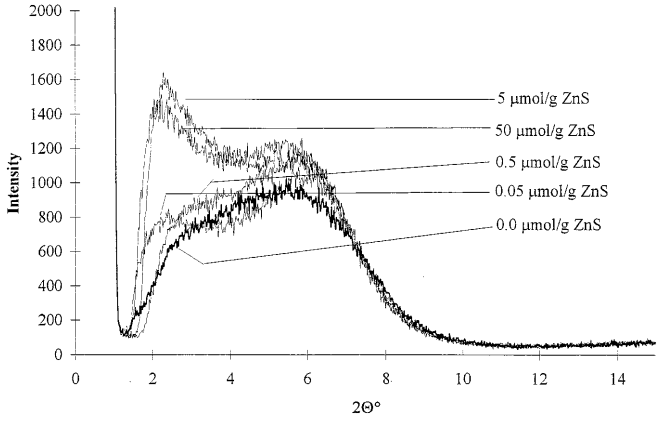

Fig. 13 XRD pattern of ZnS/hectorite nanocomposite powder at different surface precursor ion concentrations

Table 3 Basal spacings of the clay minerals in the presence of ZnS and CdS nanoparticles

Layer silicate:	Optigel			
$c_{ZnS}(\mu mol/g)$	0.05	0.5	5	50
d_L (nm)	5.6	5.0	5.3	4.6
Layer silicate:	Laponite			
$c_{ZnS}(\mu mol/g)$	0.05	0.5	5	50
d_L (nm)	3.7	3.6	3.8	4.0
Layer silicate:	Laponite			
$c_{CdS}(\mu mol/g)$	0.05	0.5	5	50
d_L (nm)	3.4	3.6	4.0	5.6

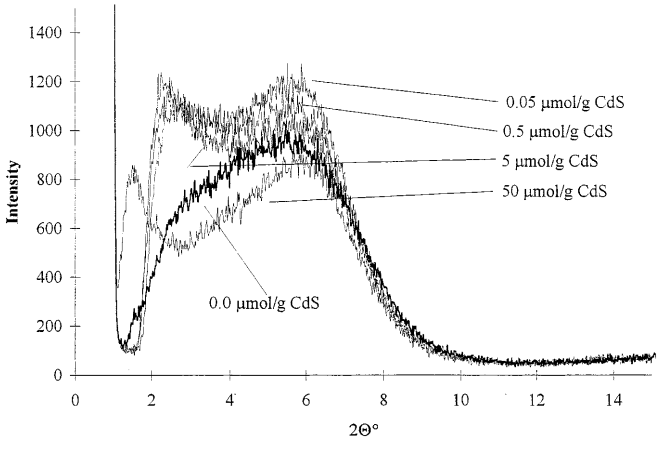

Fig. 14 XRD pattern of CdS/hectorite nanocomposite powder at different surface precursor ion concentrations

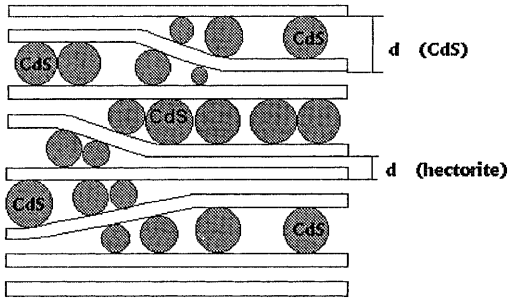

Fig. 15 The two-phase nanoparticle/clay mineral system

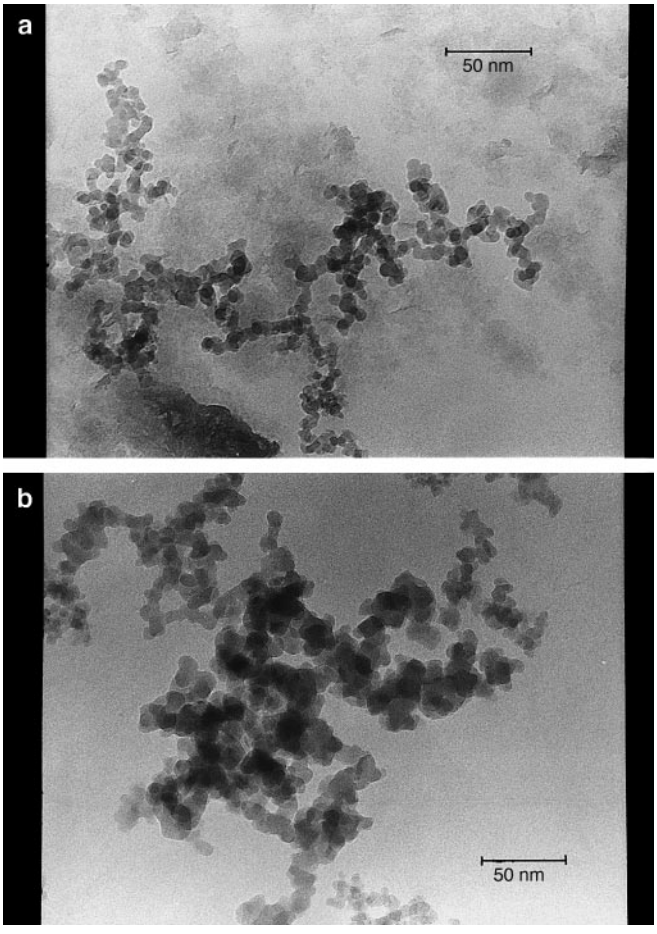

Fig. 16 Transmission electron microscopy (*TEM*) pictures of **a** 50 μmol CdS/g hectorite and **b** 50 μmol CdS/g Aerosil R972

pictures, the particle sizes of CdS on Optigel are in the range 5–10 nm. The effect of different surface hydrophobicity is seen in Fig. 18. At higher hydrophilicity (white columns on the diagram) bigger particles are formed, and the size distribution of hydrophobic aerosil particles shifted towards the smaller-size range. The fact that, in contrast to the UV/Vis measurements, larger particle diameters are obtained results from the pre-

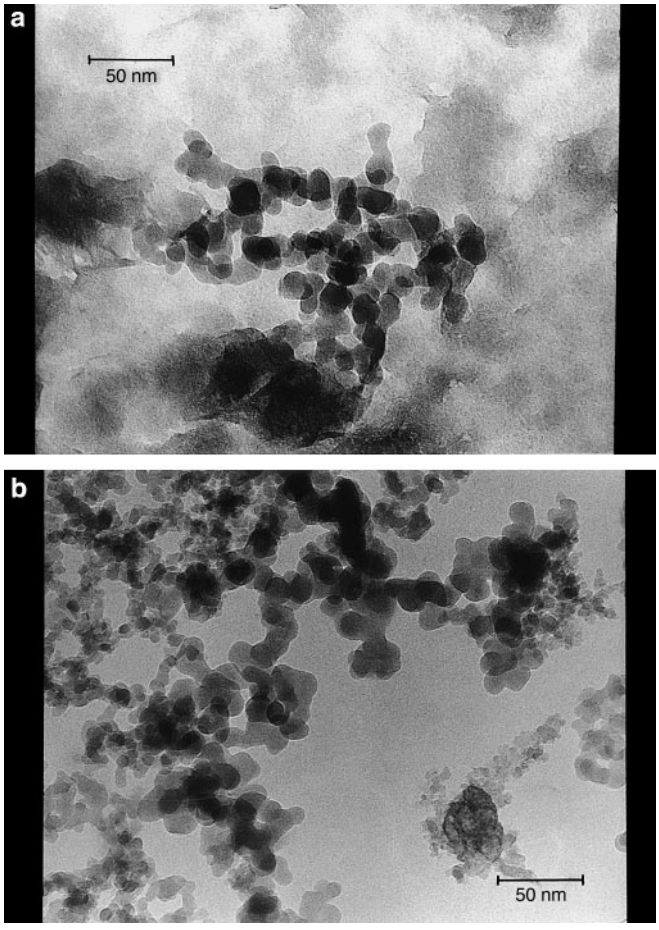

Fig. 17 TEM pictures of **a** 50 μmol ZnS/g hectorite and **b** 50 μmol ZnS/g Aerosil R972

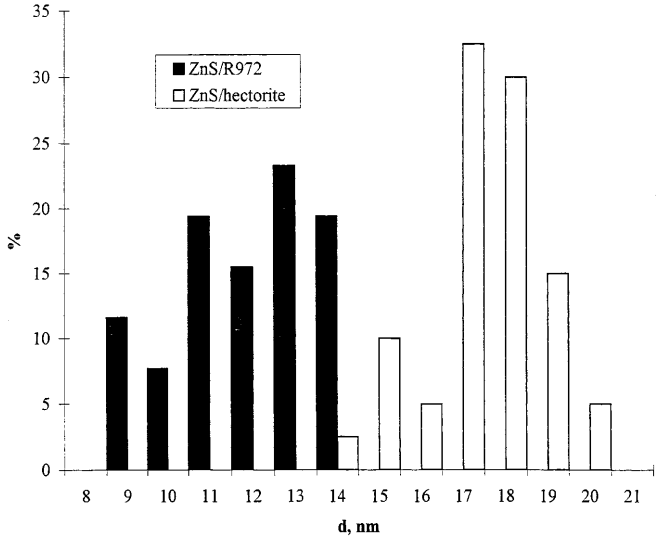

Fig. 18 Histogram of ZnS nanoparticles on hydrophilic (hectorite) and hydrophobic (R972) supports

treatment mentioned previously as well as from the tendency of metal sulphide subcolloids to form aggregates in the absence of stabilizers. Nevertheless, it can be established that our systems exhibit the expected nanophase network structure even after aggregation.

Conclusions

ZnS and CdS semiconductor nanoparticles are formed in ethanol–cyclohexane mixtures, within the solid–liquid interfacial adsorption layer rich in ethanol. The particle size is controlled by the choice of the support and by adjusting the precursor concentrations.

Rheological studies indicate that the flow characteristics of the dispersions are changed by the nanoparticles. This method is, therefore, eminently suitable for the detection of nanoparticles. On spherical SiO_2 supports the nanoparticles form interparticle bridges. When lamellar systems are applied as supports, the flow of the aqueous dispersions at pH 8.5 was Newtonian (see Refs. [30–32] for the pH dependence of the flow behaviour of sodium bentonites and montmorillonites).

UV/Vis absorption spectrophotometry is not only suitable for the reliable detection of subcolloids but also supplies valuable information on particle size via the determination of λ_g and E_g. E_g clearly depends on the concentration of the precursor ions.

Changes in the structure of the lamellar supports detected by XRD also yielded important data regarding the presence of nanoparticles. The intercalation of nanoparticles resulted in the formation of a two-phase nanostructured system. The effectiveness of the method of synthesis was verified and the physical parameters of the nanoparticles formed were determined by several independent methods.

Acknowledgements This work was supported by grants AKP 97-141 2,4 and FKFP 0402/1999 in Hungary.

References

1. Henglein A (1987) Colloid Polym Sci 73:1–4
2. Ostwald W (1916) Die Welt der vernachlassigten Dimensionen. Steinkopf, Dresden
3. Weller H, Fojtik A, Henglein A (1985) Chem Phys Lett 117–485
4. Fujishima A, Honda K (1972) Nature 238:37–38
5. Lianos P, Thomas JK (1986) Chem Phys Lett 125:299–302
6. Meyer M, Wallberg C, Kurihara K, Fendler JH (1984) J Chem Soc Chem Commun 90–91
7. Enea O, Bard A (1986) J Phys Chem 90:301–310
8. Lianos P, Thomas JK (1987) J Colloid Interface Sci 117:505–512
9. Motte L, Petit C, Boulanger L, Lixon P, Pileni P (1992) Langmuir 8:1049–1053
10. Resch U, Eychmüller A, Hasse M, Weller H (1992) Langmuir 8:2215–2218
11. Rossetti R, Hull R, Gibson JM, Brus LE (1985) J Phys Chem 82:552–559
12. Kamat PV, Dimitrijevic NM (1994) J Phys Chem 98:7665–7673
13. Kotov NA, Meldrum FC, Fendler JH, Tombácz E, Dékány I (1994) Langmuir 10:3797–3804
14. Kotov NA, Haraszti T,Túri L, Zavala G, Geer RE, Dékány I, Fendler JH (1997) J Am Chem Soc 119:6821–6832
15. Kotov NA, Dékány I, Fendler JH (l995) J Phys Chem 99:13065–13069
16. Trickot YM, Fendler JH (1984) J Am Chem Soc 106:7359–7366
17. Your HC, Baral S, Fendler JH (1988) J Phys Chem 92:6320–6327
18. Herron N, Wang Y, Eddy MM, Stucky GD, Cox DE, Moller K, Bein T (1989) J Am Chem Soc 111:530–540
19. Jentys A, Grimes RW, Gale JD, Catlow CRA (1993) J Phys Chem 97:13535–13538
20. Fendler JH, Kotov N, Dékány I (1996) In: Pelizzetti NATO ASI Series: Fine Particles Science and Technology from Micro to Nanoparticles. Kluwer, Dordrecht, pp 557–577
21. Kotov NA, Putyera K, Fendler JH, Tombácz E, Dékány I (1993) Colloids Surf A 71:317–326
22. Király Z, Dékány I, Mastalir Á, Bartók M (1996) J Catal 161:401–408
23. Dékány I, Nagy L, Turi L, Király Z, Kotov NA, Fendler JH (1996) Langmuir 12:3709–3715
24. Kortan AR, Hull R, Opila RL, Bawendi MG, Steigerwald ML, Caroll PJ, Brus LE (1990) J Am Chem Soc 112:1327–1332
25. Dékány I, Turi L, Galbács G, Fendler JH (1997) J Colloid Interface Sci 195:307–315
26. Dékány I, Turi L, Tombácz E, Fendler JH (1995) Langmuir 11:2285–2292
27. Dékány I, Nagy L, Turi L, Király Z, Kotov NA, Fendler JH (1996) Lagmuir 12:3709–3715
28. Dékány I, Turi L, Galbács G, Fendler JH (1989) J Colloid Interface Sci 213:584–591
29. Firth BA, Hunter RJ (1976) J Colloid Interface Sci 57:249–266
30. Brandenburg U, Lagaly G (1988) Appl Clay Sci 3:263–279
31. Lagaly G (1989) Appl Clay Sci 4:105–123
32. Permien T, Lagaly G (1995) Clays Clay Min 43:229–236